


## Interference between dielectronic recombination with two-electron one-photon transitions and radiative recombination

Konstantin N. Lyashchenko *Institute of Modern Physics, Chinese Academy of Sciences, Lanzhou 730000, China*Oleg Yu. Andreev *St. Petersburg State University, 7/9 Universitetskaya nab., St. Petersburg, 199034, Russia**and Center for Advanced Studies, Peter the Great St. Petersburg Polytechnic University, 195251 St. Petersburg, Russia*Deyang Yu \**Institute of Modern Physics, Chinese Academy of Sciences, Lanzhou 730000, China**and University of Chinese Academy of Sciences, Beijing 100049, China*

(Received 1 November 2019; accepted 3 March 2020; published 7 April 2020)

We have studied two-electron one-photon transitions in dielectronic recombination with H-like ions ( $Z = 5\text{--}54$ ) within *ab initio* QED theory. It was found that interference between dielectronic recombination with two-electron one-photon transitions and radiative recombination is prominent for light and medium ions being large enough for experimental observation. The interference manifests itself firstly in a sharp Fano-like resonance structure and secondly in a noticeable distortion of the photon angular distribution of the radiative recombination.

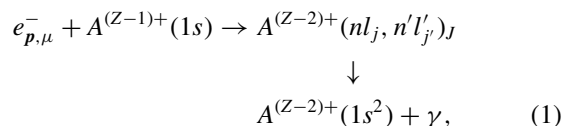
DOI: [10.1103/PhysRevA.101.040501](https://doi.org/10.1103/PhysRevA.101.040501)

Two-electron one-photon (TEOP) transition is an exotic atomic process predicted by Heisenberg about 100 years ago [1]. This is a single-photon transition proceeding in two- or more electron ions and atoms, in which two electrons simultaneously change their quantum numbers. TEOP transitions in dielectronic recombination with H-like ions are of particular interest, since the interelectron interaction plays a crucial role both for the formation of two-electron doubly excited states and for their subsequent decay to the ground state.

The first experimental evidence of TEOP was reported in [2], where the  $K\alpha\alpha$  transition ( $1s^{-2} \rightarrow (2s^{-1}, 2p^{-1})$ ) was observed in  $K$ -shell hollow Ni and Fe ions produced in heavy-ion collisions. In work [3] the same transition was observed in Mg, Al, and Si, which were doubly  $K$ -shell ionized by synchrotron radiations. The TEOP transitions, in which only one of the electrons changes its principal quantum number, while another changes only its angular quantum numbers, were studied experimentally in few-electron ions. In particular, in works [4,5] the observation of TEOP transitions ( $2s^2 \rightarrow (1s, 2p)$  and  $(1s, 2s^2) \rightarrow (1s^2, 2p)$ ) in He- and Li-like Si ions was reported. In work [6] the TEOP transitions ( $1s, 2s^2 \rightarrow (1s^2, 2p)$ ) were measured in Li-like Ar ions.

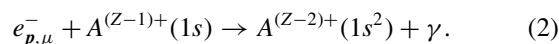
Theoretical investigations of TEOP transitions were focused on calculating the transition probabilities. Calculations of  $(2s^2) \rightarrow (1s, 2p)$  transition probabilities were carried out in [7–10]. Transitions  $(2s, 2p)_1 \rightarrow (1s^2)$  were considered in [11] for ions with  $Z \leq 28$  and in [8] for Ni. In [7–9], the calculations were performed using the GRASP code [12,13], and in [10,11] using the perturbation theory [14,15].

Dielectronic recombination (DR) provides an excellent tool for investigation of TEOP transitions in few-electron ions since an accurate theoretical description of the DR is possible [16–18] and the corresponding experimental techniques, in which the energy of the initial state can be precisely controlled, have been developed [17,19]. The DR with TEOP transitions (DR-TEOP) of H-like ions can be described as



where  $A^{(Z-1)+}$  denotes an H-like ion with nuclear charge  $Z$ . The initial state of the system is given by an incident electron  $e_{\mathbf{p},\mu}^-$  with momentum ( $\mathbf{p}$ ) and polarization ( $\mu$ ), and an H-like ion being in its ground state. The final state is an He-like ion  $A^{(Z-2)+}(1s^2)$  and a single photon  $\gamma$ . The resonant recombination proceeds via formation of a doubly excited state  $(nl_j, n'l'_j)_J$ , where  $n, l$ , and  $j$  denote the principal quantum number, the orbital momentum, and the total angular momentum of electron, respectively, and  $J$  is the total angular momentum.

DR always proceeds together with the process of radiative recombination (RR), which can be described as



It is a nonresonant process, which results in a smooth background in the electron energy-scanning spectrum when the emitted photons are counted. In the present work we show that for light and middle- $Z$  ions the interference between DR-TEOP and RR is of great importance; in particular, it significantly changes the total cross section.

\*d.yu@impcas.ac.cn

Interference between resonant and nonresonant channels leads to the Fano resonances [20,21]. The Fano-like structure for photon emission was observed experimentally in the DR with  $U^{82+\dots 90+}$  ions [22],  $Sc^{3+}$  ions [23], and  $Hg^{75+\dots 78+}$  ions [24] where the interference between DR and RR was investigated. The resonance structures of the considered processes were rather complex, which made it difficult to experimentally study the interference. We note that TEOP transitions were not noticeable in these experiments.

In this Rapid Communication we present the first study of TEOP transitions in DR with H-like ions. In contrast to many-electron ions and atoms, two-electron ions are a relatively simple system that allows both precise theoretical description within the QED theory and experimental investigation. We also show that, unlike the case of a usual two-photon DR, the interference between the RR and DR-TEOP is of particular importance, which leads to a asymmetric Fano-like profile of the cross section.

We describe the process of recombination within *ab initio* QED theory considering both RR and DR-TEOP channels in a unified and self-consistent way. The line-profile approach [25] is employed to calculate the total cross sections and the angular distribution of the emitted photons. Electron states are described by eigenvectors of the Dirac equation in which the interaction of electrons with the electric field of the nucleus is fully taken into account within the Furry picture [26]. The final basis set (*B* splines) for the Dirac equation was used for performing summation over the complete Dirac spectrum [27,28]. In the case of the TEOP transitions the contributions of the positive and negative continuum virtual states are of importance and they are taken into account using the procedure of adjusting the *B*-spline radius [29]. In the present calculations we take into account the one- and two-photon exchange corrections (and the leading part of the more-photon exchange corrections), the electron self-energy (SE), and vacuum polarization (VP) corrections [25]. The accuracy of the energy calculations is determined by the SE and VP screening corrections.

We consider the energies of incident electron covering the resonance region of *LL*-autoionizing states. So, the DR-TEOP to the ground state with *E1*-photon emission can proceed only via formation of  $(2s, 2p)_1$  states. The other states either cannot decay to the ground state with emission of a single photon (i.e., the states with zero total angular momentum) or can decay only via much weaker *E2*, *M1*, or *M2* transitions [e.g.,  $(2p, 2p)_{1,2}$  or  $(2s, 2p)_2$  states]. Thus, the contribution of these states to the one-photon recombination cross section is very small. It was found that the  $(2s, 2p_{3/2})_1$  state gives a noticeable contribution to the total cross section, while the contribution of the  $(2s, 2p_{1/2})_1$  state is barely visible. It can be understood with the fact that the TEOP transition probability for the  $(2s, 2p_{1/2})_1$  state is much smaller than one for the  $(2s, 2p_{3/2})_1$  state (e.g., for  $Ar^{16+}$  ions the ratio between these transition probabilities is about 1/178). The transition probabilities for the  $(2s, 2p_{3/2})_1$  state are presented in Table I. A similar situation holds for the *E1* transition probabilities  $(1s, 2p)_1 \rightarrow (1s^2)$  [30,31].

In Fig. 1 we present the total cross sections of one-photon recombination with  $B^{4+}$ ,  $Si^{13+}$ ,  $Ar^{17+}$ ,  $Fe^{25+}$ , and  $Xe^{53+}$  ions corresponding to the  $(2s, 2p_{3/2})_1$  resonance regions. The cross

TABLE I. The transition probabilities for decay of the  $(2s, 2p_{3/2})_1$  state to the ground state ( $W_{TEOP}$ ), the singly excited  $(1s, 2s)_0$  state (one-electron transition,  $W_{OE}$ ), and the continuum  $(1s, e_{res}^-)$  state ( $W_{Auger}$ ). The values are given in  $s^{-1}$ , and the digits in square brackets refer to the power of 10.

Ion	$W_{TEOP}$ ( $s^{-1}$ )	$W_{OE}$ ( $s^{-1}$ )	$W_{Auger}$ ( $s^{-1}$ )
$B^{3+}$	0.250 [10] 0.264 [10] <sup>a</sup>	0.341 [12] 0.358 [12] <sup>a</sup>	0.157 [15]
$Si^{12+}$	0.203 [11]	0.231 [14]	0.188 [15]
$Ar^{16+}$	0.339 [11]	0.635 [14]	0.191 [15]
$Fe^{24+}$	0.714 [11] 0.942 [11] <sup>a</sup> 0.334 [11] <sup>b</sup>	0.269 [15] 0.278 [15] <sup>a</sup> 0.265 [15] <sup>b</sup>	0.188 [15]
$Xe^{52+}$	0.300 [12]	0.382 [16]	0.162 [15]

<sup>a</sup>[11].

<sup>b</sup>[8], scaled as  $Z^2$  and  $Z^4$  from Ni for  $W_{TEOP}$  and  $W_{OE}$ , respectively.

sections exhibit sharp Fano profiles [20,21], which can be parametrized as

$$\sigma = \sigma_{RR} + \frac{2A}{\pi\Gamma q^2} \left[ \frac{(q + \epsilon)^2}{1 + \epsilon^2} - 1 \right]. \quad (3)$$

Here,  $\sigma_{RR}$  is the total cross section of the RR, which gives an almost constant background in the resonance region,  $\Gamma$  is the width of the  $(2s, 2p_{3/2})_1$  state,  $q$  is the Fano parameter describing the resonance asymmetry,  $A$  is the second parameter of the Fano interpolation, and  $\epsilon = 2(\epsilon - \epsilon_{res})/\Gamma$  is the reduced energy offset from the resonance center. The parameters characterizing the resonance structure of the cross sections are presented in Table II. Comparing the Fano parameters for DR-TEOP with those for DR presented in [24], we conclude that the DR-TEOP is characterized by the especially small Fano parameter ( $q$ ) that corresponds to very asymmetric resonance structures.

In Fig. 2 we present the total cross sections of one-photon recombination as a function of the nuclear charge ( $Z$ ) for several characteristic energies of the incident electron ( $\epsilon$ ). The RR cross section, which is represented by  $\sigma(\epsilon_{res} \pm 20\Gamma)$ , is almost constant over a wide range of  $Z$ . This is due to the fact that the RR cross section is scaled as  $Z^2/\epsilon$ , while  $\epsilon$  is scaled as  $Z^2$ . The nontrivial behavior of  $\sigma(\epsilon_{max})$  and

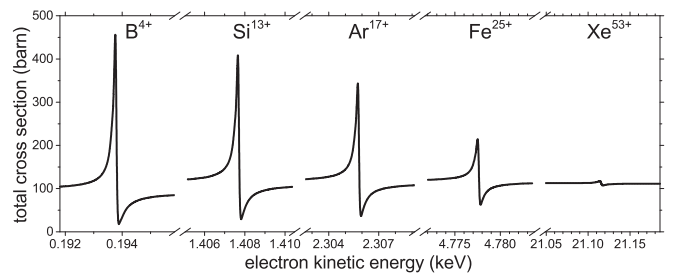


FIG. 1. One-photon recombination cross section as a function of kinetic energy of the incident electron for  $B^{4+}$ ,  $Si^{13+}$ ,  $Ar^{17+}$ ,  $Fe^{25+}$ , and  $Xe^{53+}$  ions. The resonant structures are determined by the corresponding contributions of the doubly excited state  $(2s, 2p_{3/2})_1$ .

TABLE II. The parameters characterizing the resonant structure of the cross sections for various He-like ions. The second and third columns present the energies ( $E' = E_{(2s, 2p_{3/2})_1} - 2mc^2$ ) and widths ( $\Gamma$ ) of the autoionizing  $(2s, 2p_{3/2})_1$  state. Columns 4–7 present the DR characteristic energies of incident electron: resonant energies ( $\varepsilon_{\text{res}} = E_{(2s, 2p_{3/2})_1} - \varepsilon_{1s} - m_e c^2$ ), the corresponding photon energies ( $\omega_{\text{res}}$ ), and the energy shifts corresponding to the maximum and minimum of cross sections ( $\Delta\varepsilon_{\text{max/min}} = \varepsilon_{\text{max/min}} - \varepsilon_{\text{res}}$ ). The data are given in the rest frame of the ion.

Ion	$E'$ (keV)	$\Gamma$ (eV)	$\varepsilon_{\text{res}}$ (keV)	$\omega_{\text{res}}$ (keV)	$\Delta\varepsilon_{\text{max}}$ (eV)	$\Delta\varepsilon_{\text{min}}$ (eV)
B <sup>3+</sup>	-0.1465	0.103	0.1938	0.4536	-0.03	0.10
Si <sup>12+</sup>	-1.2656	0.139	1.4077	3.8455	-0.03	0.13
Ar <sup>16+</sup>	-2.1206	0.168	2.3058	6.4266	-0.05	0.14
Fe <sup>24+</sup>	-4.5001	0.309	4.7776	13.6056	-0.11	0.22
Xe <sup>52+</sup>	-20.1851	3.463	21.1156	61.3864	-1.56	1.77

$\sigma(\varepsilon_{\text{min}})$  comes from the interference between the RR and the DR-TEOP. The energies  $\varepsilon_{\text{max}}$  and  $\varepsilon_{\text{min}}$  denote the incident-electron energies corresponding to the maximum and minimum of the total cross section, respectively. For  $Z < 10$ , the DR-TEOP channel dominates the RR, and shows almost a constant behavior of  $\sigma(\varepsilon_{\text{max}})$  and  $\sigma(\varepsilon_{\text{min}})$ . This is due to the weak dependence of the total widths ( $\Gamma \approx \Gamma_{\text{Auger}}$ ) on  $Z$ . We also can see that the DR-TEOP becomes insignificant for  $Z > 50$ . However, in the case of light and medium- $Z$  ions the total cross section is large enough ( $\sigma_{\text{max}} = 200\text{--}450$  barn) for experimental observations.

To study the DR-TEOP resonance structure, we provide a detailed analysis of the process for Ar<sup>17+</sup> ions. In the upper panel of Fig. 3 we show separately the contributions of the nonresonant channel (RR), the resonant channel (DR-TEOP), and their interference to the cross section as a function of  $\varepsilon$ . The DR-TEOP shows a Lorentz profile, which is defined by the resonant energy  $\varepsilon_{\text{res}}$  and the width ( $\Gamma$ ) of the  $(2s, 2p_{3/2})_1$  state.

In the lower panel of Fig. 3, we present the normalized differential cross section ( $\frac{1}{\sigma} \frac{d\sigma}{d\Omega_e}$ ) as a function of the polar angle  $\theta_e$  of the emitted photon for several values of the incident-electron energies:  $\varepsilon_{\text{max}}$ ,  $\varepsilon_{\text{min}}$ ,  $\varepsilon_{\text{dis}}$ , and  $\varepsilon_{\text{res}} \pm 20\Gamma$ . The photon polar angle ( $\theta_e$ ) is measured relative to the momentum of the ion in the incident-electron rest frame. At the nonresonant

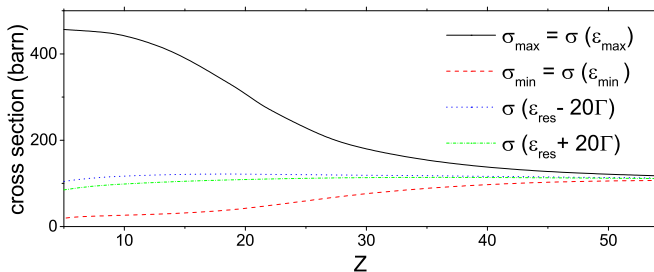


FIG. 2. Total cross section of one-photon recombination corresponding to the resonance energy region of the  $(2s, 2p_{3/2})_1$  state as a function of the nuclear charge  $Z$ . The cross sections are presented for the incident-electron energies  $\varepsilon_{\text{max}}$ ,  $\varepsilon_{\text{min}}$ , and  $\varepsilon_{\text{res}} \pm 20\Gamma$ .

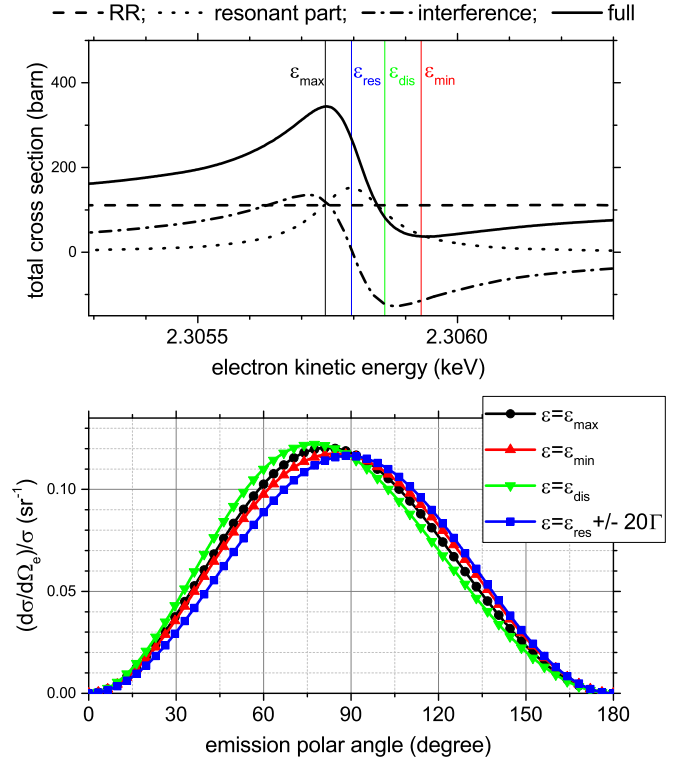


FIG. 3. Upper panel: total cross section for one-photon recombination of Ar<sup>17+</sup> ions as a function of the incident-electron kinetic energy. The contributions of the RR, the DR-TEOP, and their interference are presented separately. The electron energies corresponding to the resonance position of the  $(2s, 2p_{3/2})_1$  state ( $\varepsilon_{\text{res}}$ ), the maximum and the minimum of the total cross section ( $\varepsilon_{\text{max}}$  and  $\varepsilon_{\text{min}}$ ), and the strongest distortion of the angular distribution ( $\varepsilon_{\text{dis}}$ ), are indicated by vertical lines. Lower panel: normalized differential cross section ( $\frac{1}{\sigma} \frac{d\sigma}{d\Omega_e}$ , in  $\text{sr}^{-1}$ ) in the incident-electron rest frame for the collision energies of  $\varepsilon_{\text{max}}$ ,  $\varepsilon_{\text{min}}$ ,  $\varepsilon_{\text{dis}}$ , and  $\varepsilon_{\text{res}} \pm 20\Gamma$ .

energies  $\varepsilon = \varepsilon_{\text{res}} \pm 20\Gamma$ , the differential cross section exhibits a well known  $\sin^2 \theta_e$  angular distribution, which originates from the RR [32,33]. However, in the resonance (between  $\varepsilon_{\text{max}}$  and  $\varepsilon_{\text{min}}$ ) we can see a considerable distortion of the  $\sin^2 \theta_e$  angular distribution, which reaches its maximum value at  $\varepsilon_{\text{dis}}$ .

In the ion rest frame the DR-TEOP photons fit the  $\sin^2 \theta_i$  angular distribution, where  $\theta_i$  is the photon polar angle in this frame. Such a rather simple angular distribution originates from the fact that only one doubly excited state  $[(2s, 2p_{3/2})_1]$  makes a considerable contribution to the DR-TEOP. The  $(2s, 2p_{3/2})_1 \rightarrow (1s^2)$  TEOP transition proceeds with emission of a  $E1$  photon with the projection of the total angular momentum  $M = 0$ . The photons with  $M = \pm 1$  are emitted only if the electron spin-flip takes place, which is strongly suppressed for the low- and middle- $Z$  ions. The  $E1$  ( $M = 0$ ) transition determines the  $\sin^2 \theta_i$  angular distribution of the DR-TEOP photons in the ion rest frame. In the incident-electron rest frame the following formula can be employed:

$$\frac{d\sigma}{d\Omega_e} \approx \frac{3}{8\pi} \left| \sqrt{\sigma_{\text{RR}}} \sin \theta_e e^{i\delta_{\text{RR}}} + \frac{f(\varepsilon) \sin \theta_e}{\gamma^2 (1 - \beta \cos \theta_e)^2} \right|^2, \quad (4)$$

where  $\sigma_{\text{RR}}$  is the total cross section of RR, and  $\gamma = 1/\sqrt{1 - \beta^2}$  is the Lorentz factor ( $\beta$  is the collision velocity

TABLE III. Parameters of the approximations of the total and differential cross sections given by (3)–(7). Parameters of the Fano profile ( $q$  and  $A$ ) are presented in the second and third columns. Parameter  $\beta$  gives the resonant collision velocity in the relativistic units. Parameter  $a$  is introduced in Eq. (7). The values of  $\sigma_{RR}(\varepsilon_{\text{res}})$  and  $\sigma_{DR}(\varepsilon_{\text{res}})$  are the corresponding cross section calculated at the resonance energies  $\varepsilon_{\text{res}}$  (in barn). The last column shows the accuracy of the approximation (4) defined as  $|\frac{d\sigma}{d\Omega} - \frac{d\sigma^{\text{approx}}}{d\Omega}| / \frac{(\sigma_{RR} + \sigma_{DR})}{4\pi}$ .

Ion	$q$	$A$	$\beta$	$a$	$\sigma_{RR}(\varepsilon_{\text{res}})$	$\sigma_{DR}(\varepsilon_{\text{res}})$	Accuracy
$B^{3+}$	-2.38	0.061	0.0275	0.033	82	287	$\leq 3\%$
$Si^{12+}$	-1.96	0.049	0.0741	0.100	107	213	$\leq 3\%$
$Ar^{16+}$	-1.77	0.038	0.0947	0.129	111	152	$\leq 4\%$
$Fe^{24+}$	-1.41	0.016	0.1358	0.190	114	45	$\leq 4\%$
$Xe^{53+}$	-1.21	0.001	0.2789	0.421	115	3	$\leq 7\%$

in the relativistic units). The first term in approximation (4) represents the  $\sin^2 \theta_e$  angular distribution of the RR in the incident-electron rest frame. The second term corresponds to the  $\sin^2 \theta_i$  angular distribution of the DR-TEOP in the ion rest frame being Lorentz transferred to the incident-electron rest frame. The function  $f(\varepsilon)$  depends only on the collision energy and defines the Lorentz profile of the pure DR-TEOP channel

$$f(\varepsilon) = \frac{\Gamma}{\varepsilon - \varepsilon_{\text{res}} + i\frac{\Gamma}{2}} = \sqrt{\frac{\sigma_{DR}(\varepsilon_{\text{res}})}{\varepsilon^2 + 1}} e^{i\delta_{DR}}, \quad (5)$$

where  $\sigma_{DR}(\varepsilon_{\text{res}})$  corresponds to the maximum value of the DR-TEOP Lorentz profile.

The interference of RR and DR-TEOP channels depends on their relative phase  $\delta = \delta_{DR} - \delta_{RR}$ . The DR-TEOP phase can be approximated as

$$\delta_{DR} = \pi - \text{arccot}(\varepsilon). \quad (6)$$

The energy dependence of the  $\delta_{DR}$  can be also obtained within the Fano formalism [20]. For the RR phase we found that the angular dependence can be written with high accuracy as

$$\delta_{RR} = a \cos \theta_{\beta/2} = a \frac{\beta/2 - \cos \theta_e}{1 - \beta \cos(\theta_e)/2}, \quad (7)$$

where  $\theta_{\beta/2}$  is the photon polar angle in the frame moving with velocity  $\beta/2$  regarding the ion rest frame (it is measured relative to the momentum of the incident electron);  $a$  is a smooth function of the collision energy which can be regarded as a constant in the resonant region. We note that the relative phase  $\delta$  grows with increasing of collision energy becoming equal to  $\pi/2$  in the narrow energy region between minimum and maximum of the Fano profile.

In the approximation (4) we neglect the contributions of the higher multipoles of the emitted photon for the DR-TEOP and spin flip of the captured electron. Hence, it provides a good accuracy in the case of low- and middle- $Z$  ions. The values of the approximation parameters as well as the accuracy of the approximation (4) are presented in Table III. We note that in the small energy region between the Fano maximum and minimum of the cross section where it decreases dramatically (see Fig. 1) the accuracy of the approximation can exceed the presented in Table III values reaching 9% for  $B^{4+}$ ,  $Si^{13+}$ , and  $Ar^{17+}$  and 15% for  $Fe^{25+}$  and  $Xe^{53+}$ .

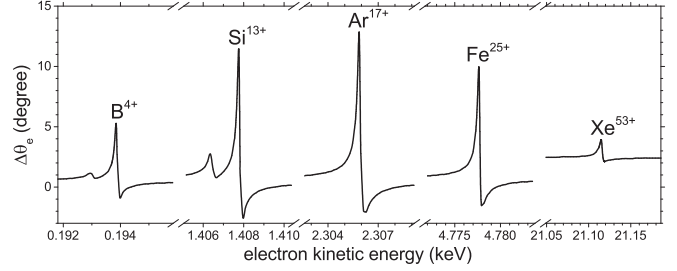


FIG. 4. The angular shift ( $\Delta\theta_e = 90^\circ - \theta_e^{\text{max}}$ ) as a function of the incident-electron kinetic energy for various ions. The polar angle  $\theta_e^{\text{max}}$  is determined by the maximum of the normalized differential cross section ( $\frac{1}{\sigma} \frac{d\sigma}{d\Omega_e}$ ) in the incident-electron rest frame.

The angular distortion (see the lower panel of Fig. 3) can be characterized by the angular shift  $\Delta\theta_e = 90^\circ - \theta_e^{\text{max}}$ , where  $\theta_e^{\text{max}}$  is the position of the maximum of the angular distribution in the incident-electron rest frame. In Fig. 4 we present the angular shift  $\Delta\theta_e$  as a function of the incident-electron kinetic energy. First, the energy dependence of the  $\Delta\theta_e$  has explicit resonance structure similar to that of the total cross sections (see Fig. 1). The main contribution to the  $\Delta\theta_e$  is given by the  $(2s, 2p_{3/2})_1$  doubly excited state, and the smaller peak at the left corresponds to the contribution of the  $(2s, 2p_{1/2})_1$  state. The smaller peak is shown for boron and silicon ions; however, it is not seen for the heavier ions because it is located beyond the presented energy regions. Second, the angular shift  $\Delta\theta_e$  demonstrates a strong  $Z$  dependence, which differs from the  $Z$  dependence of the total cross section (see Fig. 1). On the one hand the angular distortion is a relativistic effect that disappears in the nonrelativistic limit [see (4) with  $\beta \rightarrow 0$ ]. On the other hand, in the case of high  $Z$ , the DR-TEOP is strongly suppressed by the RR channel, and this explains the decrease of  $\Delta\theta_e$  for high  $Z$  ions. Figure 4 also demonstrates that the DR-TEOP can be studied by measuring the photon angular distribution of the one-photon recombination. The angular shift can be quite large in the resonance region; in particular, it reaches  $13^\circ$  for the  $Ar^{17+}$  ion.

In summary, TEOP transitions in one-photon recombination with H-like ions are studied within *ab initio* QED theory. Strong interference between the DR-TEOP and the RR leads to a prominent Fano-like resonance structure in the total cross section. The DR-TEOP manifests itself also in the distortion of the  $\sin^2 \theta_e$  angular distribution, which is typical for the RR process. In the  $LL$  resonance group, only one doubly excited state  $[(2s, 2p_{3/2})_1]$  contributes significantly to the DR-TEOP process. Hence, the differential cross section can be parametrized with the use of the Fano formalism and interpolation of the angular dependence of the DR-TEOP and RR amplitude phase factors. The total cross sections ( $\sigma_{\text{max}} = 200\text{--}450$  barn) and the distortion of the angular distributions (the angular shift is up to  $13^\circ$ ) are large enough for experimental observation at heavy-ion storage rings available in the GSI (Darmstadt, Germany) and the Institute of Modern Physics (Lanzhou, China).

The authors are indebted to Dr. A. Gumberidze for reading the manuscript and making valuable remarks. We are also

grateful to Qiong Yang, Jizheng Duan, and Jibo Li from Heavy Ion Research Facility at Lanzhou (HIRFL) for their help with using the supercomputer clusters. This work is supported by the National Key Research and Development Program of China under Grant No. 2017YFA0402300, the National Natural Science Foundation of China under Grant No. 11774356, and the Chinese Academy of Sciences (CAS)

President's International Fellowship Initiative (PIFI) under Grant No. 2018VMB0016. The work of O.Y.A. was partly supported by the Ministry of Education and Science of the Russian Federation under Grant No. 3.1463.2017/4.6. The work of K.N.L. and O.Y.A. on the calculation of the energies and widths was supported solely by the Russian Science Foundation under Grant No. 17-12-01035.

- 
- [1] W. Heisenberg, *Z. Phys.* **32**, 841 (1925).
- [2] W. Wölfl, C. Stoller, G. Bonani, M. Suter, and M. Stöckli, *Phys. Rev. Lett.* **35**, 656 (1975).
- [3] J. Hosszowska, J.-C. Dousse, J. Szlachetko, Y. Kayser, W. Cao, P. Jagodziński, M. Kavčič, and S. H. Nowak, *Phys. Rev. Lett.* **107**, 053001 (2011).
- [4] R. Elton, J. Cobble, H. Griem, D. Montgomery, R. Mancini, V. Jacobs, and E. Behar, *J. Quant. Spectrosc. Radiat. Transfer* **65**, 185 (2000).
- [5] F. B. Rosmej, H. R. Griem, R. C. Elton, V. L. Jacobs, J. A. Cobble, A. Y. Faenov, T. A. Pikuz, M. Geißel, D. H. H. Hoffmann, W. Süß, D. B. Uskov, V. P. Shevelko, and R. C. Mancini, *Phys. Rev. E* **66**, 056402 (2002).
- [6] Y. Zou, J. R. Crespo López-Urrutia, and J. Ullrich, *Phys. Rev. A* **67**, 042703 (2003).
- [7] D. Zhang, C. Dong, and K. Fumihiko, *Chin. Phys. Lett.* **23**, 2059 (2006).
- [8] L. Natarajan and R. Kadrekar, *Phys. Rev. A* **88**, 012501 (2013).
- [9] L. Natarajan, *Phys. Rev. A* **90**, 032509 (2014).
- [10] F. Goryaev, L. Vainshtein, and A. Urnov, *At. Data Nucl. Data Tables* **113**, 117 (2017).
- [11] U. I. Safronova and V. S. Senashenko, *J. Phys. B* **10**, L271 (1977).
- [12] F. Parpia, C. Fischer, and I. Grant, *Comput. Phys. Commun.* **94**, 249 (1996).
- [13] P. Jönsson, X. He, C. F. Fischer, and I. Grant, *Comput. Phys. Commun.* **177**, 597 (2007).
- [14] V. Shevelko and L. Vainshtein, *Atomic Physics for Hot Plasmas* (Institute of Physics Publishing, Bristol, 1993).
- [15] L. Vainshtein and U. Safronova, *At. Data Nucl. Data Tables* **21**, 49 (1978).
- [16] O. Yu. Andreev, L. N. Labzowsky, and A. V. Prigorovsky, *Phys. Rev. A* **80**, 042514 (2009).
- [17] D. Bernhardt, C. Brandau, Z. Harman, C. Kozhuharov, A. Müller, W. Scheid, S. Schippers, E. W. Schmidt, D. Yu, A. N. Artemyev, I. I. Tupitsyn, S. Böhm, F. Bosch, F. J. Currell, B. Franzke, A. Gumberidze, J. Jacobi, P. H. Mokler, F. Nolden, U. Spillman, Z. Stachura, M. Steck, and T. Stöhlker, *Phys. Rev. A* **83**, 020701(R) (2011).
- [18] K. N. Lyashchenko and O. Y. Andreev, *Phys. Rev. A* **91**, 012511 (2015).
- [19] N. Nakamura, A. P. Kavanagh, H. Watanabe, H. A. Sakaue, Y. Li, D. Kato, F. J. Currell, and S. Ohtani, *Phys. Rev. Lett.* **100**, 073203 (2008).
- [20] U. Fano, *Phys. Rev.* **124**, 1866 (1961).
- [21] U. Fano and J. W. Cooper, *Phys. Rev.* **137**, A1364 (1965).
- [22] D. A. Knapp, P. Beiersdorfer, M. H. Chen, J. H. Scofield, and D. Schneider, *Phys. Rev. Lett.* **74**, 54 (1995).
- [23] S. Schippers, S. Kieslich, A. Müller, G. Gwinner, M. Schnell, A. Wolf, A. Covington, M. E. Bannister, and L.-B. Zhao, *Phys. Rev. A* **65**, 042723 (2002).
- [24] A. J. González Martínez, J. R. Crespo López-Urrutia, J. Braun, G. Brenner, H. Bruhns, A. Lapiere, V. Mironov, R. Soria Orts, H. Tawara, M. Trinczek, J. Ullrich, and J. H. Scofield, *Phys. Rev. Lett.* **94**, 203201 (2005).
- [25] O. Yu. Andreev, L. N. Labzowsky, G. Plunien, and D. A. Solovyev, *Phys. Rep.* **455**, 135 (2008).
- [26] W. H. Furry, *Phys. Rev.* **81**, 115 (1951).
- [27] W. R. Johnson, S. A. Blundell, and J. Sapirstein, *Phys. Rev. A* **37**, 307 (1988).
- [28] V. M. Shabaev and V. A. Yerokhin, *Phys. Rev. Lett.* **88**, 091801 (2002).
- [29] V. A. Yerokhin, A. Surzhykov, and A. Müller, *Phys. Rev. A* **96**, 042505 (2017).
- [30] W. R. Johnson, D. R. Plante, and J. Sapirstein, *Adv. At., Mol., Opt. Phys.* **35**, 255 (1995).
- [31] O. Yu. Andreev, L. N. Labzowsky, and G. Plunien, *Phys. Rev. A* **79**, 032515 (2009).
- [32] J. Eichler, A. Ichihara, and T. Shirai, *Phys. Rev. A* **51**, 3027 (1995).
- [33] J. Eichler and T. Stöhlker, *Phys. Rep.* **439**, 1 (2007).